

Low Mass Ratio Hydrofoil Flutter Experimental Model Design Procedure

MARINE 2021

O.D'Ubaldo^{1,*}, C.M. Rizzo¹, D.Dessi² and F.Passacantilli²

¹ Dipartimento di Ingegneria Navale, Elettrica, Elettronica e delle Telecomunicazioni – DITEN
Università degli Studi di Genova (UNIGE)
Via All'Opera Pia, 11 A, 16145 Genova GE, Italy. E-mail: olivia.dubaldo@edu.unige.it,
cesare.rizzo@unige.it

² Institute of Marine Engineering (CNR-INM)
National Research Council of Italy
Via di Vallerano 139, 00128 Rome, Italy. E-mail: daniele.dessi@cnr.it, fabio.passacantilli@inm.cnr.it

* Corresponding author: Olivia D'Ubaldo, olivia.dubaldo@edu.unige.it

ABSTRACT

The present paper describes the design concept and specifications of a hydrofoil model to be actually tested for flutter experimental analysis at CNR-INM Institute of Marine Engineering towing tank in Rome. The design procedure is the result of concurrent application of numerical and analytical approaches: CAD models are used for geometrical modelling and mass properties calculations, FEM is employed to calculate model stiffness, natural frequencies and verify model strength, and Theodorsen analytical approach is implemented to predict flutter velocity. Theodorsen approach allows calculating the flutter condition as a function of physical parameters as geometries, mass and stiffness, assuming two-dimensional, incompressible aerodynamic coefficients and sinusoidal harmonic motion at flutter instability condition (zero damping condition).

As first step, the authors built a broad literature review upon past flutter experimental experiences in both air and water flow focusing on the troubles linked to the increase of flow density and viscosity, the technical issues to be considered when designing the flutter model and setting up experimental campaigns. Most of the flutter experimental campaigns reported in the literature deal with high mass ratio models as aerofoils operating in light, low viscosity fluids; less common are experimental reports about low mass ratio models as light hydrofoils.

The sample design process started by a dynamical scale of a hydrofoil model, flutter-tested in 1971, chosen as main reference. The model is designed to encounter flutter at a speed compatible with the range of velocity imposed by the water tank facilities. The combination of design parameters is optimised to meet facilities speed range, construction issues and Theodorsen approach application field.

Keywords: hydrofoil; flutter; low mass ratio; experimental; Theodorsen ;

NOMENCLATURE

μ	Mass ratio [-]
m	Structure mass per unit span [Kg/m]
S	Static mass moment about elastic axis per unit length [Kg]
I_α	Structure mass moment of inertia per unit length [Kg m]
h	Heave motion [m]
\dot{h}	Heave acceleration [m s ⁻²]
α	Pitch motion [rad]
$\ddot{\alpha}$	Pitch acceleration [rad s ⁻²]
K_h	Bending stiffness per unit span [N/m]
K_α	Torsional stiffness per unit span [Nm/rad]
ρ	Fluid density [kg m ⁻³]
$l(t)$	Lift force [N]
$m(t)$	Fluid dynamic moment [N m]
t	Time variable [s]
ω	Oscillation frequency [rad/s]
V	Flow velocity [m/s]
c	Foil chord [m]
b	Foil semi-chord [m]
C_l	2D Lift coefficient [-]
w	Downwash velocity [m/s]
k	Reduced frequency [rad/s]
ω_h	Bending natural frequency [Hz]
ω_α	Torsional natural frequency [Hz]
X_α	Non-dimensional distance between CE and CG [-]
r_α	Non-dimensional radius of gyration [-]
ω_{ratio}	Bending to torsional natural frequency ratio
a	Non-dimensional distance from CE to mid-chord
CE	Elastic Centre
CG	Centre of Gravity
LE	Leading Edge
TE	Trailing Edge
CRP	Carbon Reinforced Plastic

1. INTRODUCTION

Wing flutter is an aeroelastic instability well-known in the aeronautic field since the beginning of the 20th century, while the appearance of similar phenomena in hydrofoils started to worry naval architects just few decades ago. This is firstly due to the fact that flutter occurrence is less common in hydrofoil, since this kind of appendages, apart from propeller blades, traditionally operate at relatively low speed. At the same time, it should be considered that flutter theoretical evaluation and experimental validation are more challenging when operating in water: studying fluid-structure interaction phenomena becomes a more complicated issue when considering a heavy, viscous fluid as the water, and more sophisticated models are needed.

As first step, the authors carried out a comprehensive literature review upon past flutter experimental tests on 2D foil sections in both air and water flow, focusing on the technical issues to be considered when designing the flutter experimental model and setting up the experimental campaign, with particular reference to the differences between air and water testing. A key parameter in flutter sensitivity analysis is the mass ratio μ which is the ratio between structure and fluid densities, accounting for the ratio between fluid and solid inertial effects affecting the fluid structure interaction. Most of the flutter experimental campaigns reported in literature deal with high mass ratio physical models as aerofoils operating in light, low viscosity fluids, while less common in literature are experimental reports about low mass ratio models as light hydrofoils. The density of a wing structure is always largely greater than the density of the surrounding air-flow: the mass ratio μ is therefore relatively high. When dealing with a problem of fluid-structure interaction in water, which has a density 1000 times greater than air, the operative values of μ drop drastically, especially when considering hydrofoils built with light, composite materials.

The previous considerations point out that hydrofoil flutter has not been extensively studied from an experimental point of view not only because it is a rare event in ship engineering, but also because flutter testing in water is much more challenging for several reasons. Nonetheless, this phenomenon has received some consideration in some unexpected onset of vibrations of appendages, possibly due to low-damping conditions in the pre-critical instability regime. Thus, in the present paper, the authors present the design of a hydrofoil model conceived to verify the possibility of flutter occurrence within the velocity limits imposed by facility constraints. The model will then be flutter-tested in the towing tank facility of Consiglio Nazionale delle Ricerche - Istituto di Ingegneria del Mare (CNR-INM) in Rome.

As a numerical tool to establish that the flutter will really occur, Theodorsen's theory of a bidimensional wing sections in potential flows is employed. In this way, the dependency of the flutter speed from structural variables has been investigated, and an optimal combination of design parameters has been selected compatibly with several design constraints. In Theodorsen's theory, the foil structure is simply represented through a limited set of parameters: structural mass, inertia and stiffness, position of centre of gravity and elastic axis, and aspect ratio. Thus, one of the main tasks for using Theodorsen's theory as a flutter verification tool, is to reduce the 3D representation of the hydrofoil to a 2D model. In the simplified 2D model, a critical role is played by the bending and torsional natural frequencies of the hydrofoil, which have been calculated by means of FEM modal analysis. Though the main attention is devoted in choosing the structural parameters which will allow for flutter below the maximum carriage speed, other aspects like the correct alignment of hydrofoil with the inflow or the measurement equipment have been also of concern and will be dealt within the paper, along with indications on the planned experimental procedure for determining the flutter velocity.

2. REFERENCE EXPERIMENTAL FLUTTER CAMPAIGNS

A comprehensive literature review of past works concerning flutter testing of foils in both air and water was preliminary carried out, and allowed the authors to have an overview on the technical issues to be considered when designing the physical model and the other components of the experimental set-up and to understand the troubles linked to the increase of flow density and viscosity. Most of the flutter experimental campaigns reported in literature deal with high mass ratio models as aerofoils operating in light, low viscosity fluids, while less common are experimental reports about light hydrofoils. It is worthwhile considering the following statement from (Caporali & Brunelle, 1964), which points out the difficulties related to using experimental results to validate theoretical models: *‘While flutter theory has generally failed to predict experimental results, (Baird et al., 1962), (H.N. Abramson & Langner, 1964; Rowe & Marvin, 1968), flutter experiments as well have often failed to produce usable results in the form of flutter occurrences ((Herr, 1961; Kaplan & Lehman, 1966)). In cases where some agreement has been obtained between theory and experiment, the data have been insufficient to confirm theoretical predictions over a range of mass ratio values and the theories have lacked general applicability or self-consistency’.*

The experimental campaign carried out by Abramson & Ransleben, (1965) has been chosen as main reference for flutter model and experimental set-up design, because of compatibility with the intention of the authors and completeness and accuracy of the experimental report. They built a 0.99 mass ratio hydrofoil which was flutter-tested at David Taylor Model Basin. In (H. Norman Abramson & Ransleben, 1965) important details upon construction issues are given, including design parameters choice, experimental set up and testing procedure, and experimental outputs recording. The results provided in (H. Norman Abramson & Ransleben, 1965) were considered and discussed by Besch & Liu (1971). Using Abramson and Ransleben work as reference, they generated a series of flutter models to explore the effect of mass ratio μ variation on flutter limit state. Technical details of the construction, assembling and testing of the models reported in (Besch & Liu, 1971) are also extensively provided in (Guido Ransleben & Antonio Houston, 1970).

Despite the present work focuses on low mass ratio hydrofoil flutter experimental evaluation, the authors considered also lesson learned from aeronautical literature to investigate the dependency of flutter phenomenon from the physical variables. In particular Woolston and Castile technical report (1951) has been deeply analysed even if it treats higher mass ratio aerofoil.

3. THEODORSEN THEORY

The theory has been firstly published in 1934 as a purely theoretical NACA technical report (Theodorsen, 1935) providing a theoretical approach to calculate the flutter limit speed of a aerofoil section, given the surrounding fluid density and its structural characteristics. Few years later, Theodorsen and Garrick published another technical report (1940) where the theory was further defined from a practical point of view, giving some clarifications about its application. The effect of the different parameters on the flutter limit and the comparison with several experimental data were also provided. This simple mathematical model is still valid in giving preliminary indications about the stability analysis of foils with simple geometry, and it often represents a reference case for more sophisticated simulations.

The assumptions at the basis of Theodorsen theory are the following:

- Incompressible, inviscid, attached, unsteady flow
- Flat wake

- Flat plate geometry, as a limit representation of symmetrical, small thickness wing sections
- Small motion amplitude

The approach solves a 2-dof linear unsteady fluid-elastic system, where the dofs are heave or plunge (h) and pitch (α) of a reference point of the typical section, as shown in Fig.1

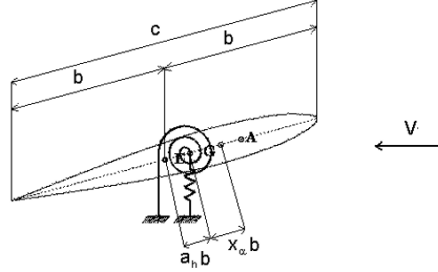


Figure 1.Foil typical section.

If heave and pitch are referred to the elastic axis of the typical section (point E in Fig. 1), the differential system describing the motion is:

$$\begin{pmatrix} m & S \\ S & I_\alpha \end{pmatrix} \begin{Bmatrix} \ddot{h} \\ \ddot{\alpha} \end{Bmatrix} + \begin{pmatrix} K_h & 0 \\ 0 & K_\alpha \end{pmatrix} \begin{Bmatrix} h \\ \alpha \end{Bmatrix} = \begin{Bmatrix} -l(t) \\ m(t) \end{Bmatrix} \quad (1)$$

where:

- m is the structure mass per unit span
- I_α is the structure torsional mass inertia per unit span
- $S = X_\alpha m b$ is the static mass moment per unit span
where: $X_\alpha = (\text{distance between CE and CG})/\text{semichord}$
 b is the semi-chord length
- $K_h = \omega_h^2 * m$ is the bending stiffness per unit length
Where: ω_h is the structure bending natural frequencies
- $K_\alpha = \omega_\alpha^2 * I_\alpha$ is the torsional stiffness per unit length
where: ω_α is the structure torsional natural frequencies
- $l(t)$ is the time dependent lift force
- $m(t)$ is the time dependent hydrodynamical moment about the elastic axis

It is worth recalling that, in the limit that the typical section represents an 3D wing, heave and pitch can be interpreted as the amplitudes of the spanwise out-of-plane bending and torsional modes. When flutter occurs, the total damping of the foil vanishes, and the motion can be assumed harmonic as it follows:

$$\alpha = \alpha_0 e^{i\omega t} \quad (2a)$$

$$h = h_0 e^{i\omega t} \quad (2b)$$

where:

- ω is the oscillation frequency
- t is the time variable

By substituting the relations in Eqs. 2a and 2b, into Eq. 1, the system becomes:

$$\begin{pmatrix} -\omega^2 m + K_h & -\omega^2 S \\ -\omega^2 S & -\omega^2 I_\alpha + K_\alpha \end{pmatrix} \begin{Bmatrix} h_0 \\ \alpha_0 \end{Bmatrix} e^{i\omega t} = \begin{Bmatrix} -l(t) \\ m(t) \end{Bmatrix} \quad (3)$$

As seen above, the functions $l(t)$ and $m(t)$ represent the fluid loading and change in time through the body motion. Theodorsen function $C(k)$ is used as a filter function to take into account the unsteadiness of the flow in the lift calculation, hence the dependency of lift generation from the oscillating frequency. The reduced frequency k gives a non-dimensional definition of the system frequency, expressed as the number of oscillations undergone by the foil during the time taken to the flow to travel across a semi-chord length ($k = \frac{\omega b}{c}$) (Wright & Cooper, 2014).



Figure 2. Theodorsen function transfer.

Thus, the unsteady lift $l(t)$ and moment $m(t)$ can be expressed as a function of $C(k)$ where k is the reduced frequency.

Since $C(k)$ includes the dependency of both lift phase and amplitude, it is a complex function and can be expressed as the sum of two function $F(k)$ and $G(k)$, representing respectively its real and imaginary parts (Eq. 4).

$$C(k) = F(k) + iG(k) \quad (4)$$

The trends of the two functions are characterised by a combination of Hankel functions of the second kind as reported in Eq. 5 and in Fig.3. At $k = 0$ (quasi-steady case), the imaginary part of Theodorsen function, $G(k)$, representing the phase lag, tends towards zero and the real part $F(k)$, representing the amplitude reduction due to unsteadiness, assume a unity value. The amplitude of lift oscillations decreases with increasing motion frequency, while the phase lag firstly increases up to a value of $k = 0.3$, and then it drops again for higher frequencies.

$$C(k) = \frac{H_1^{(2)}(k)}{H_1^{(2)}(k) + i H_0^{(2)}(k)} \quad (5)$$

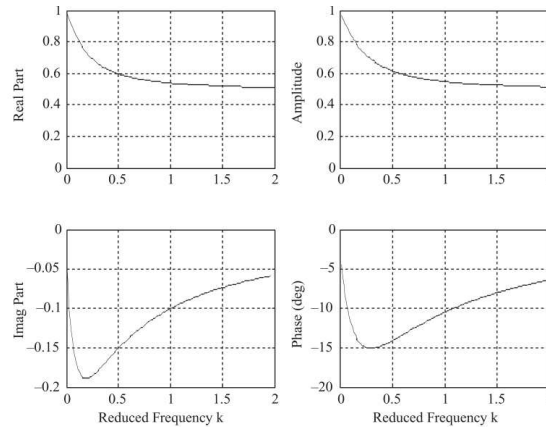


Figure 3. Theodorsen function real and imaginary part.

To solve the system, the determinant of the system coefficient matrix is imposed equal to zero and solved over speed and frequency. At that condition, the damping vanishes and the structure will experience flutter.

The physical parameters involved in the computation of Theodorsen theory are:

- Foil chord: c
- Foil CE and CG position
- Structure mass per unit span: m
- Structure torsional mass inertia: I_α
- Structure bending and torsional natural frequencies: ω_h and ω_α
- Fluid density: ρ

Therefore, the output of Theodorsen analytical model are the speed and the frequency at which the structure experiences flutter instability.

3.1. Sensitivity Analysis

The analytical model has been implemented in Matlab™ software in order to study the dependency of the flutter limit from the involved variables and to optimise the design process.

Fluid-structure interaction is a highly non-linear problem and, in the case of flutter speed calculation by means of Theodorsen's theory, the involved variables are dependent by each other.

Hence, when studying the effect of each variable on flutter speed, it should be remembered that for a different combination of the fixed parameters, the dependency from the studied variable is affected.

For this reason, the sensitivity analysis has been iterated during the design process, at each time that a flutter parameter was fixed for construction issue, as explained in Section 5. In the present paper, only the results of the last iteration of sensitivity analysis are presented, since they referred to the final model to be tested experimentally.

In addition, it should be remembered that varying one parameter at a time allows understanding the behaviour of the variables one by one, but gives out a non-realistic output. To explain that, let us go through an example: if the position of the centre of gravity (CG) is changed, the mass inertia of the model changes as well, and with it the torsional natural frequency and the frequency ratio. Studying the effect of the CG movement on flutter speed, alone, is therefore not realistic if the other dependent variables are kept fixed. Nevertheless, this type of analysis is of key importance for phenomenon understanding and it permits to give a direction to the model optimisation process.

In Table 1 it is shown the combination of parameters chosen for the optimised model. In the following subsection it is discussed the effect of changing these parameters one by one. Before going further, it should be stated that the parameters reported in Table 1, do not account for the mass of the carbon fibre shell described in Section 5.4. The authors intentionally decided to neglect this mass for preliminary calculations. This choice allows a margin on the estimated total mass which compensate the uncertainty on the effective lead density (for the calculation of ballast mass, the density of pure lead 11.34 t/m^3 has been used, however the lead employed for ballast manufacturing might contain impurities which lower the effective density). In this way, if the ballast mass will result lightly lower than the preliminary estimation reported in this paper, the addition of the shell mass, will compensate the unwanted μ lowering, otherwise, if the employed lead will result to be fairly pure, the addition of the shell mass will further increase μ , inducing a favourable condition for flutter velocity estimation. In any case, the mass of the shell is sensible to construction performance and it can be estimated to be around 280 g.

Table 1. Optimised model parameters.

GEOMETRY	Span (s)	[m]	0.533
	Chord (c)	[m]	0.152
	X_α	[-]	0.519
	S	[Kg]	0.698
	r_α^2	[-]	0.48
	I_α	[Kg m]	0.049
	a	[-]	-0.5
MASS	μ	[-]	0.97
	ζ	[-]	1.03
	m	[Kg/m]	17.66
	Total mass	[Kg]	9.42
FREQUENCY	ω_h	[Hz]	5.4
	ω_α	[Hz]	9.9
	ω_{ratio}^2	[-]	0.296

3.1.1. Relative Mass Ratio Variation

Although in Theodorsen theory it appears the variable ζ , defined as the ratio between the mass of a unit length cylinder of fluid having the chord as diameter and the mass of a unit length of the structure, in this section the authors preferred to consider the inverse of ζ ($\mu = 1/\zeta$), considering it to be more intuitive to study problem sensitivity.

From Fig. 4 it is clear that for μ greater than about 2, a linear dependency of the flutter speed from the mass ratio exists; for $\mu < 2$ the theoretical results diverges toward $V = \infty$: this result suggests the application limit of Theodorsen theory for the studied structure. For this reason, the authors designed a model with the highest mass ratio, in order to allow experimental vs. theoretical comparison. Despite all the available internal volume of the model is designed to be full of lead, the maximum reachable μ resulted to be 0.97. The flutter limit estimated with Theodorsen for the current model then represents just a reference value, and the trend of the linear part of the curve can be used to preview the effective flutter speed of the sample. Once experimental results will be available, it will be possible to properly comment the behaviour of Theodorsen outcomes. It is remembered that for a different model (e.g. different mass inertia or different frequency ratio) the curve V vs. μ is shifted but the trend is similar.

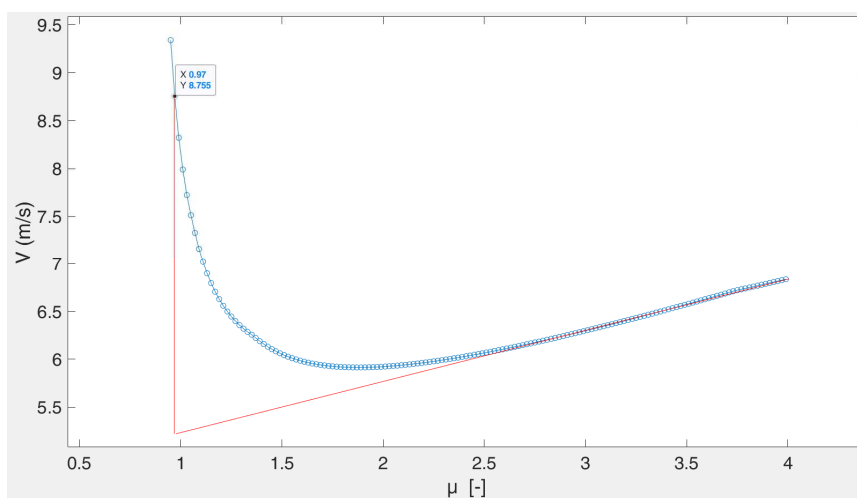


Figure 4. Dependency of flutter velocity by μ .

3.1.2. Elastic Axis Position Variation

The parameter a is defined as the distance from the elastic centre (CE) to mid-chord, divided by the semi-chord (b). The parameter is negative if the CE is located in the front half of the profile, as often happens in hydrofoils, positive if it is located in the rear part, toward the TE. In Fig 5 it can be noticed that moving the CE toward mid-chord reduces the flutter speed of the model. However, the authors decided to keep CE as close as possible to the centre of hydrodynamic pressure, in order to avoid divergence occurrence, which for light hydrofoil, might anticipates flutter.

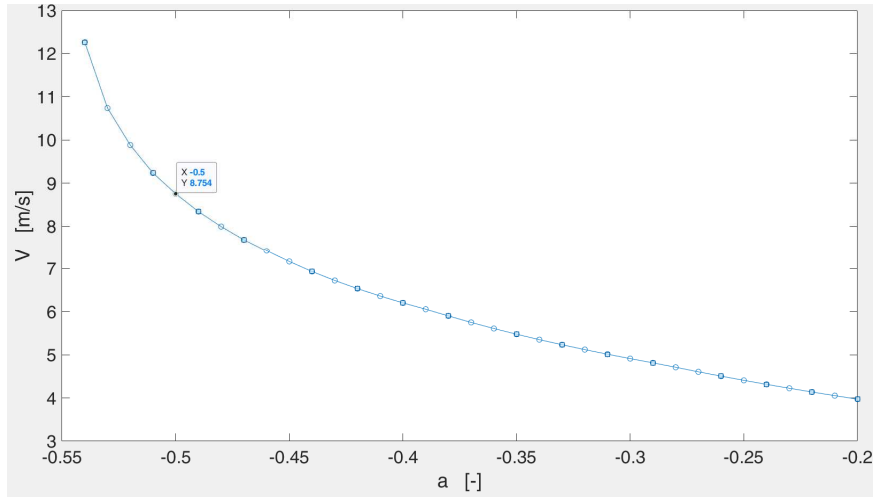


Figure 5. Dependency of flutter velocity by parameter a .

It should also be remarked that moving the CE have a double effect, which does not appear in Fig. 5: moving CE toward mid-chord, the distance between CE and CG (X_α) is reduced as well, with an effect on the flutter speed discussed in Section 0.

3.1.3. Centre of Gravity Position Variation

The distance between CE and CG, made nondimensional with respect to the semi-chord length, is indicated as X_α . Having constrained the position of CE as discussed in the previous section, the parameter X_α is governed by the position of the CG of the foil.

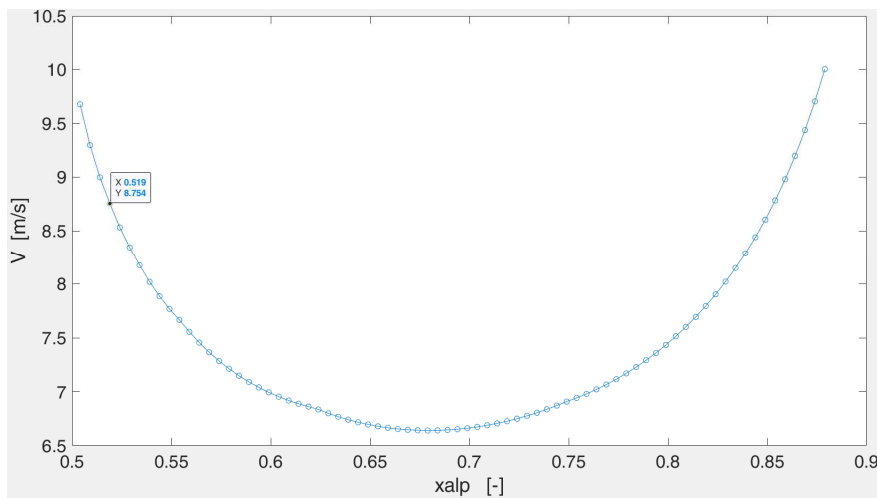


Figure 6. Dependency of flutter velocity by X_α .

In Fig. 6 it is clear that moving the CG toward the Trailing Edge (TE) would have determined a lower flutter limit, and therefore in a more convenient solution for the aim of the design process described in the present paper. However, because of the shape of the NACA profile, and because of the need of filling the whole internal volume of the foil with ballast to reach the highest μ , it was not possible to further move back the CG. The choice of the NACA 16-012 profile is indeed justified by the fact that the maximum thickness is located at 50% of the chord from the LE, allowing a relatively high value of X_α .

The V vs. X_α curve of the discussed model presents a minimum at $X_\alpha = 0.68$. However it should be remembered that for different models (e.g. different CE, mass inertia or different frequency ratio) the trend of the curve would be the same but the tangency point would be shifted.

3.1.4. Radius of Gyration Variation

The radius of gyration allows to establish a relation between the mass and the mass inertia of a rotating body. It is defined as the distance from the elastic axis to an imaginary point where it should be concentrated the whole mass of the body to deliver the actual mass inertia of the structure: it is therefore an index of mass distribution.

In Theodorsen theory, the radius of gyration has a key role in flutter limit calculation, and it is employed in non-dimensional form as it follows:

$$r_\alpha^2 = \left(\frac{I_\alpha}{m b^2} \right) \quad (6)$$

One of the driving principles of the design process presented in this paper, is the maximisation of the hydrofoil mass, aimed to increase the mass ratio μ and, as a consequence, the reliability of theoretical results as discussed in Section 3.1.1. However, from the results of Fig 7. it is clear that the distribution of the mass in the structure should be such as the mass inertia is maximised as well. Since the authors decided to give priority to the maximisation of the variable μ , the available internal volume of the model ended up to be full of lead, making the variable r_α^2 almost a fixed parameter, for a given shape of the NACA 16-012 profile, as it happened for the variable X_α .

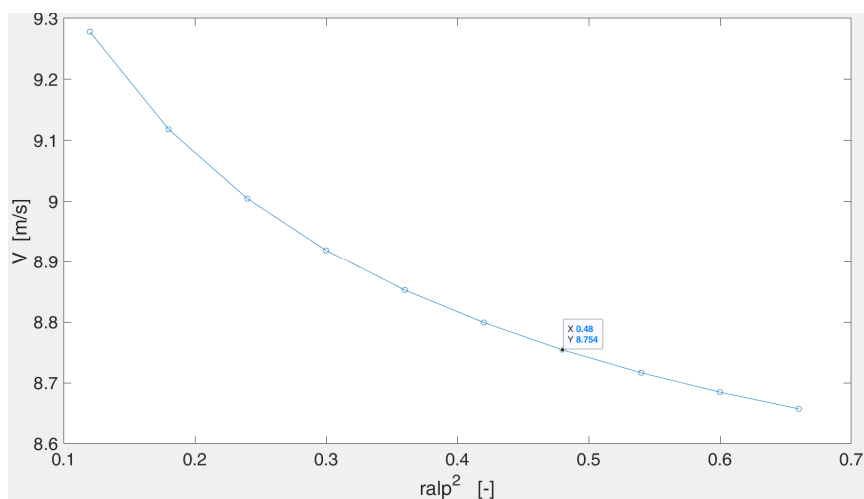


Figure 7. Dependency of flutter velocity by r_α^2 .

3.1.5. Frequency Ratio Variation

The higher is the ratio between bending and torsional natural frequency, the lower is the flutter limit speed. These frequencies depends on the bending and torsional stiffness of the structure, as well as on the mass and mass inertia of the model as discussed later in Section 5.

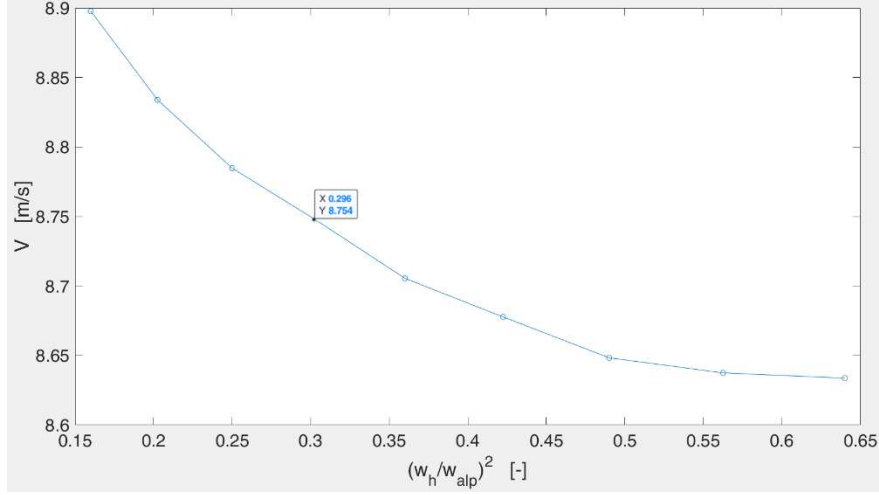


Figure 8. Dependency of flutter velocity by ω_{ratio} .

Being mass and mass inertia governed by the maximisation of the mass ratio μ , the variable ω_{ratio} is controlled by means of the elastic beam cross section and span as detailed in Section 5.1. Because of the shape of the NACA 16-012 profile, and the chord-wise position of the elastic axis, ω_{ratio} resulted to be the parameter characterised by the highest freedom of choice: beam cross section and span have been therefore adapted at the end of the iterative design optimisation process, to the combination of the others variables, imposed by construction issues, to reach the desirable flutter speed.

3.1.6. Torsional Natural Frequency Variation

Beside the dependency of the flutter solution from the frequency ratio, the torsional natural frequency ω_α itself appears in the calculation of the flutter speed reported Eq. 7, showing the linear dependency plotted in Fig. 9 (Theodorsen, 1935), (Theodorsen & Garrick, 1940).

$$V(h) = \frac{(r_\alpha \times \omega_\alpha \times b)}{\sqrt{ki}} \times \frac{1}{k} \times \frac{1}{X_{flutter}} \quad (7)$$

Where $\frac{1}{k}$ and $\frac{1}{X_{flutter}}$ are function of ω_{ratio} among others .

It follows that for a fixed bending frequency ω_h , an increase in ω_α has a double effect in flutter speed reduction: in other words, for a fixed delta of ω_{ratio} , it is more incisive to lower ω_α , rather than increase ω_h .

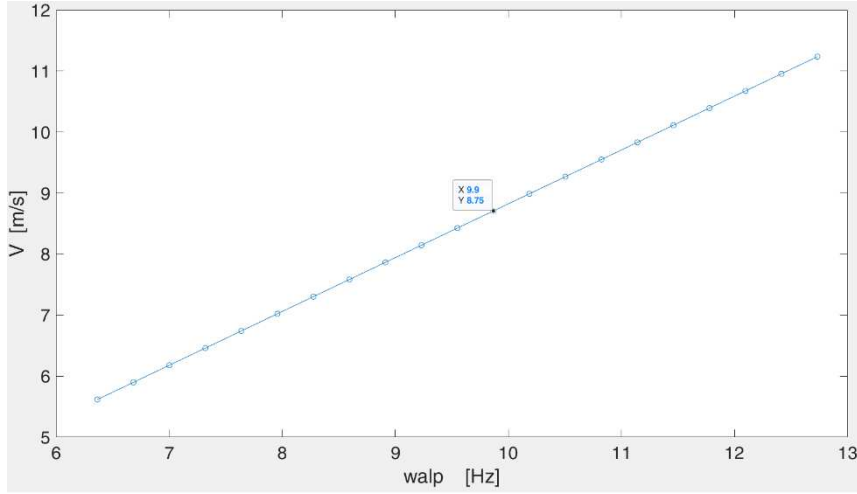


Figure 9. Dependency of flutter velocity by ω_{α} .

4. FLUTTER MODEL DESIGN CRITERIA

The authors designed their own hydrofoil model so as to experience flutter below the velocity of 15 m/s imposed by the towing tank carriage speed limit. Theodorsen theoretical approach allowed us to evaluate the effect of different design parameters on the flutter limit speed and represented the guideline to choose the combination of model stiffness, geometries and mass distribution optimised to obtain the lowest flutter speed and the highest relative mass ratio μ . The tricky side of the design process lies in the fact that the flutter limit speed is a non-linear function of a series of parameters, which depend by each other. Each flutter variable affects directly and indirectly the limit speed. Since the flutter limit is directly proportional to the chord dimension, and the maximum operating speed of the towing tank is relatively low for flutter occurrence, it was necessary to reduce as much as possible the size of the model compatibly with construction issues, in order to encounter flutter instability during the trials. Beside construction issues, the small size of the model also limited the internal volume of the model representing a limit for the total specific mass of the hydrofoil reachable by filling the sample with lead as described in Section 5.2. As discussed in the previous section, the specific mass (m) of the structure is a very significant value as it affects the mass ratio ($\mu = m/\pi \rho b^2$), which in turn affects the flutter speed, as well as the accuracy and reliability of the theoretical results. The design process started by a dynamic scale of a NACA 16-012 with 0.99 mass ratio flutter tested hydrofoil model chosen as reference from the literature (H. Norman Abramson & Ransleben, 1965). Besch & Liu, (1971) proved experimentally the reliability of the flutter model dynamical scale process described in the following for a generic scale factor n :

- $\mu_n = \mu_{parental}$ (the scale process works if fluid density remains the same)
- To guarantee that the hydrodynamic forces keep similarity after the scaling process, the flutter frequency has to remain constant
- To obtain $V_{flutter,n} = n V_{flutter,parental}$, the following condition on the chord is imposed:
- $b_n = n \times b_{parental}$ (same relation worth for all geometrical parameters)
- Since the specific mass (Kg/m) is proportional to b^2 , ($m = \mu (\pi \rho b^2)$), it follows that :
- $m_n = n^2 m_{parental}$
- Since the mass (Kg/m) is imposed to be $m_n = n^2 m_{parental}$, and $L_n = n L_{parental}$, it follows :
- $(EI, GJ)_n = n^6 (EI, GJ)_{parental}$ (condition on stiffnesses)
- Natural frequencies are not affected by the scaling process

It follows that scaling the chord of the model of a certain factor, keeping μ constant, leads to an equal scaling of the flutter speed: this principle has been applied to investigate the suitable scale factor to apply to the parental reference flutter model to adapt it to the current facilities carriage limit. However, a too small-scale factor would have been necessary to reach an useful speed.

The authors therefore decided to fix the scale factor to reach a useful chord size in terms of construction issues and changed some parameters of the sample to further anticipate the flutter occurrence: in this way the authors moved away from the ‘comfort zone’ of predictable experimental flutter speed guaranteed by the reference. This represents a possible risk, since Theodorsen theoretical approach overestimates the flutter limit proportionally to the combination of structural parameters. Having changed this combination, the authors cannot know in advance how much the theoretical approach overestimate the flutter limit velocity.

The offsets of the profile are kept constant to NACA 16-012 geometry in order to keep the knowledge of a standard profile with known fluid dynamical properties, and also to minimise the difference between the current and the reference experimental campaigns.

The relative mass ratio has been kept as much as possible close to the reference value 0.99 considering it to be “*small enough to demonstrate behaviour in the range of interest to hydrofoil applications, but large enough to insure that flutter would occur.*” (H. Norman Abramson & Ransleben, 1965). The reference value was also chosen by Abramson and Ransleben (1965) as the limit of reliability of Theodorsen theory: for lower value of mass ratio, the analytical outcome exponentially diverged from the experimental results; however it should be remarked that this limit value varies with the characteristic of the model, as already detailed in Section 3.1.1.

The position of the elastic centre is kept the same of the reference model since $EA \equiv c/4$, represents the theoretical condition of $V_{divergence} = \infty$, assuming the hydrodynamical forces to act at $c/4$. This is a condition of interest since for a low mass ratio hydrofoil, the divergence instability might occur before the flutter, falsifying the intention of the experimental campaign.

The distribution of the lead ballast mass inside the volume of the foil affects directly a series of parameters, which in turn affect the flutter limit: the lead distribution alteration changes the chord wise position of the centre of gravity (X_α) and the radius of gyration (r_α), which defines the lead mass inertia, which in turn affect the torsional natural frequency (ω_α). The latter is also dependent by the torsional stiffness (GJ); if the torsional natural frequency changes, also the frequency ratio ω_h / ω_α changes, for a certain structure. It can be concluded that the mass distribution affects directly four of the Theodorsen flutter variables: X_α , r_α , ω_α , and therefore the ratio ω_h / ω_α ; because of these two last terms, the mass distribution also affects indirectly torsional and bending stiffness of the structure (EI and GJ).

Then, having fixed the chord and the specific mass, as explained earlier, and having chosen structure and ballast materials, the best distribution of lead is found searching the maximum distance between CG and CE and the maximum value of torsional mass inertia, which leads to the minimum torsional frequency ω_α . Final goal is to choose a combination of distribution of mass/beam cross section which leads to the minimum flutter speed.

To anticipate the instability, the Aspect Ratio of the sample has been increased from 5 to 7 inducing lower ω_h , and lower ω_α : it should be noticed that the increase in span affects the bending stiffness more than the torsional stiffness; therefore, fixing EI and GJ, the higher is the aspect ratio, the lower is the frequency ratio (ω_h / ω_α); Since the effect of the linear dependency of flutter speed on ω_α is stronger than the effect of inverse dependency on frequency ratio (ω_h / ω_α), it follows that the longer is the span, the lower is the effective flutter speed. It should also be noticed that, the higher is the aspect ratio, the closer are experimental

and analytical outcomes, as confirmed in (Woolston & Castile, 1951). This is probably due to the fact that the longer is the foil span, the more consistent is the 2D assumption in fluid-dynamical forces evaluation.

5. NACA 16-012 FLUTTER MODEL DESIGN PROCESS

The design process was driven by the criteria defined in Section 4, and supported by the concurrent application of numerical and analytical approaches: CAD models are used for geometrical modelling and mass properties calculations, FEM is employed to calculate model stiffness, natural frequencies, and verify model strength, and the analytical approach allows for flutter velocity prediction.

For better control of the design parameters, the structure of the elastic foil is conceived in a way that each component has a specific role. Thus, the foil flexibility is almost entirely provided by its elastic backbone beam, while the hydrodynamic load is transferred to the backbone using segmentation of the foil surface, which in turn is attached to the backbone only in few points. This concept design simplifies also the overall design, as it reduces the mutual interaction between components and also guarantees a better analogy with the reduced order FEM model and therefore a more rigorous comparison between experimental and numerical results.

The required bending and torsional stiffness of the whole model are provided by a H-beam spar running along the foil span, and all the others structural components are assembled avoiding participation to the overall stiffness: to do that, the model is segmented spanwise in a series of strips separated by a gap of 1 mm; the only point of contact of these strips with the beam is a chord wise aluminium web per strip, fixed to the beam and bonded to the ballast as better described in Section 5.4. The ballast is then defined as *floating* since it does not directly touch neither the beam nor the shell and therefore it is supposed not to add stiffness to the whole structure. Its role is then to purely add inertial properties to the model. Same principle works for the Carbon Reinforced Plastic (CRP) shell, which has a double purpose: provide external shape and fairing of the profile and making watertight each strip.

5.1. H- Beam Design and Modelling

The aluminium H-beam is responsible for the overall stiffness of the model.

The cross section of the beam is chosen to be H-shaped for two reasons: it is the standard shape that better adapts to the NACA profile and it is the cross section which better allows bending and torsional stiffness tuning. The thickness of the standard profile NACA 16-012 represents the limit for the transversal (thickness wise) dimension of the H-beam cross section, while web and core thicknesses have been chosen to provide the optimal combination of bending and torsional stiffness.

It is worth to recall that the model optimisation process is aimed to lower the flutter limit of the hydrofoil model keeping the dimension of the sample reasonable from a construction point of view, e.g., not too small or too large.

As described in Section 3.1, the lower is the torsional frequency (ω_α), the lower is the flutter speed, and the higher is the ratio between bending and torsional natural frequencies (ω_h/ω_α), the lower is the flutter velocity.

Bending stiffness is related to bending natural frequency and torsional stiffness is related to torsional frequency as it follows in Eq 8:

$$\omega_h = \sqrt{\frac{K_h}{m}} \quad \omega_\alpha = \sqrt{\frac{K_\alpha}{I_\alpha}} \quad (8)$$

To lower ω_α , the mass inertia of the whole model should be maximised, and the H-beam cross section core thickness should be minimised, taking care of the torsional yielding limit state, and milling issues. Since the margin for mass inertia adaptation resulted to be very small, because of lead maximum filling of the sample internal volume, the torsional stiffness (i.e. the H-beam cross section core thickness) has been chosen after having defined the ballast mass distribution.

The thickness of the H-beam cross section webs has been considered as the parameter to adjust bending stiffness and control the frequency ratio.

The beam has been modelled with FE elements in order to obtain a reduced order model for natural frequencies evaluation and FSI simulations. The spar is modelled with beam elements assigning H cross section with chosen geometries and aluminium properties. Refers to Section 5.4 for beam cross section dimensions.

5.2. Inertial Considerations

As already discussed, a design objective is to keep the value of relative mass ratio as much as possible close to the reference value $\mu = 0.99$ since for lighter structures the flutter occurrence becomes unpredictable by means of Theodorsen theory. To reach such a value of mass ratio, the gap between ballast and beam should have been filled with lead, but this solution was not compatible with the design principles.

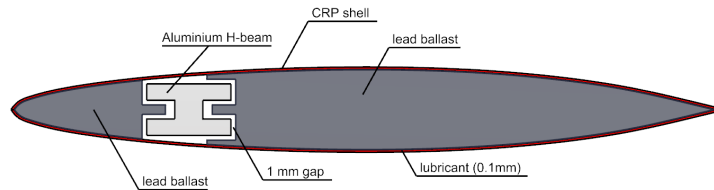


Figure 10. Model generic transversal section.

The best compromise has been found to dedicate most of the internal volume of the sample to the ballast, allowing inter-parts tolerances, aluminium beam structure and composite shell thickness: although a greater distance between CG and CE would induce a lower flutter speed, the authors did not have significant tolerance in choosing the mass distribution, and X_α ended to be an ‘almost-fixed’ parameter, reducing Theodorsen variables control. The ballast of each strip is divided into two front blocks, at the LE, and two aft block in the rear part of the profile. To gain volume, both front and aft ballasts blocks are extended between the webs of the beam, allowing 1 mm gap all the way around to avoid contact with the beam itself: this choice increased significantly the complexity of lead casting process to realise the ballast (See Fig. 11).

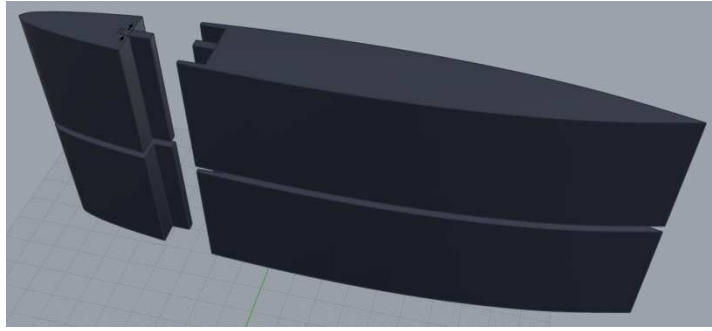


Figure 11. Lead ballast blocks.

No gap (0.1 mm) is left between the lead and the CRP shell in order to keep the value of $\mu > 0.97$, but suitable lubricant will be spread at the interface instead of bonding. For the same reason, the gap between each of the eight strips of model is reduced at 1 mm, assuming it as the minimum useful value: the larger is the gap, the more empty volume is included in the mass calculation, and the lower gets the mass ratio. Again, for the same reason, the external shell is realised in CRP to allow the lowest thickness without losing stiffness: the thinner is the shell, the less volume is allocated to a light CRP instead of the heavy lead.

Per each block of ballast, considering lead density, the mass inertia referred to the projection of the volume centroid on the elastic axis, has been obtained by means of a CAD software: to add these masses and inertias in the FE reduced order model, a series of 32 mass point has been modelled along the beam line, and characterised with each block inertial properties; the inertial contribution of the 8 aluminium frames is taken into account analogously.

The overall mass inertia of the model allows calculating the radius of gyration r_α necessary to compute Theodorsen theory.

The CG of the model, including all component's masses, is located at 39.52 mm behind the elastic axis. The nondimensional parameter X_α resulted then to be 0.519.

5.3. Frequency Analysis

The vibration modes of the FE representation of the hydrofoil have been computed using FEM software ADINATM. The natural frequencies of the relevant modes for flutter analysis depend on mass, inertia and stiffness: for this reason the structural model employed for frequency calculation, should properly reflect the stiffness of the elastic beam and the inertial properties of each block of ballast. As already introduced in previous sections, the slender structure is modelled by means of beam elements having aluminium properties and two nodes per element, with free-clamped boundary conditions at the ends. In particular, it is rigidly constrained at one side to simulate the attachment to the carriage and the ballast blocks are modelled as lumped masses located along the elastic axis taking into account the inertial increment due to CG-CE offset.

ADINA identifies the natural modes of vibrations of the structure by means of Eigenvalue modal analysis.(ADINA R & D, 2016)

As stated previously, the main concern is here to extract the low-frequency transversal (out-of-plane) bending mode and torsional modes., whose frequencies feed the Thoedorsen's model.

The lower natural frequency resulted to be 5.4 Hz, associated to a vibration mode almost entirely participated by a pure out-of-plane bending mode of the cantilever beam as shown in Fig. 12 The vibration mode at 9.9 Hz is instead mainly contributed by a pure torsional mode (see Fig. 13). An in-plane bending mode also

exists at 7.1 Hz, which is weakly coupled with the other modes and is disregarded in the Theodorsen's flutter model.

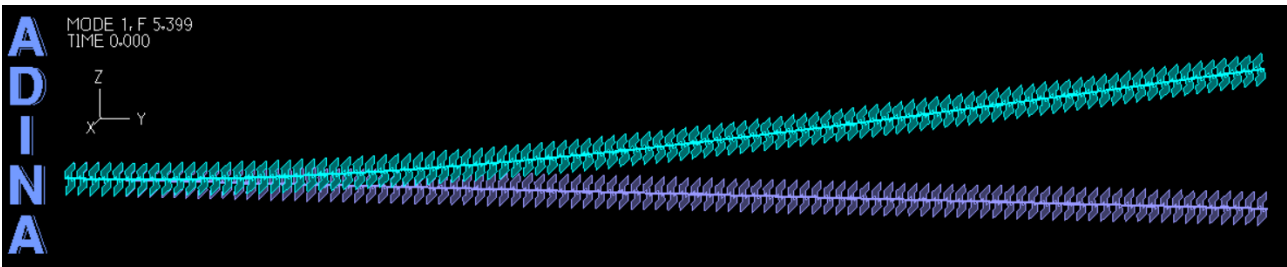


Figure 12. Bending natural mode of vibration.

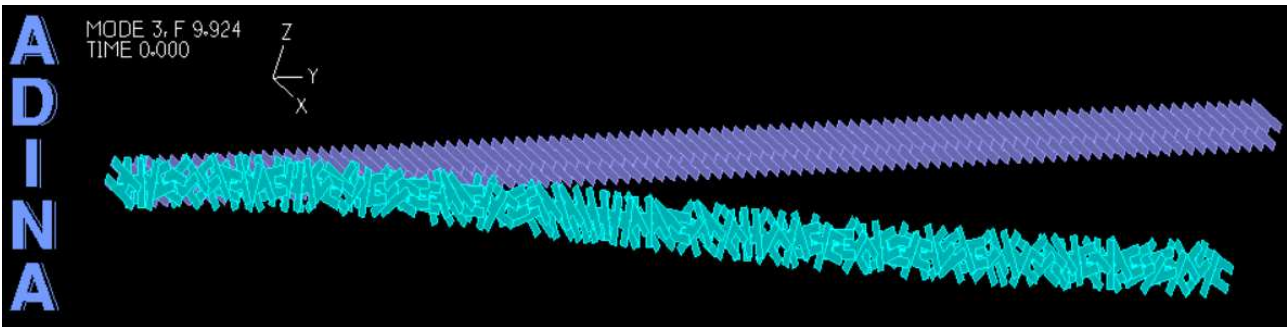


Figure 13. Torsional natural mode of vibration.

5.4. Structural Components and Assembling

In this section, the authors propose a summary of model components, providing details on construction and assembling issues.

The sample is segmented in eight rigid strips held together by a span-wise elastic beam which provide model stiffness.

The flutter model is composed by:

- Aluminium H-beam
- Aluminium transversal webs x 8
- Lead ballast divided in 32 blocks
- CRP shell segmented in 8 strips

The elastic beam is milled from an aluminium bar: the head of the beam, which has rectangular solid cross section (see Fig.14), is clamped in the towing tank carriage facilities support (see Section 6), making this part stiff enough to consider it to be rigid: in this way, the reduced order model employed for analytical and numerical evaluation, simulates the elastic behaviour of the foil span, constrained at the point where it gets in contact with the carriage support.

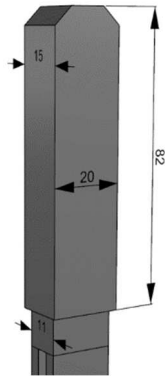


Figure 14. H-beam head.

The upper part of the beam is not included in the reduced order model as it is assumed to be rigid. The elastic part of the beam is milled with H cross section having the dimensions reported in Fig.15 chosen following the principles expressed in Section 5.1.

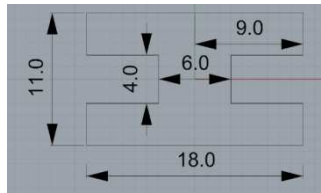


Figure 15. H-beam cross section.

The choice of using aluminium instead of steel for beam construction, is due to the fact that, to provide the same bending and torsional stiffness with steel, webs and core would have resulted very thin, inducing a more complex milling process. The elastic beam is eventually 532 mm long.

The eight transversal webs are equally spaced along this length and fixed to the beam by means of epoxy bonding: their function is to support the ballast of each model strip and transmit the inertial loads to the beam. (See Fig. 16)

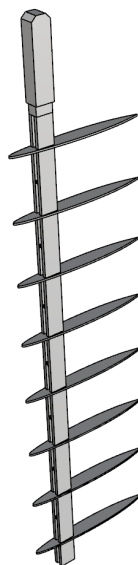


Figure 16. H-beam with ballast supporting webs.

The webs are laser cut from a 2 mm aluminium plate.



Figure 17. Aluminium web.

The first step of model assembling is to couple the beam with the webs.

Beside the manufacturing of beam and webs, the model production process foresees the casting of the ballast blocks and the construction of the CRP shell. Each model strip is ballasted by four blocks of lead, sized as described in Section 5.2: they are bonded to the upper and lower sides of each web, ahead and behind the beam (see Fig. 18)



Figure 18. H-beam with fixed lead ballast .

Each strip is enveloped by a 0.5 mm thick CRP shell, built in two halves, laminated and consolidated under vacuum on a female mould realised with a 3D printer on NACA 16-012 profile.

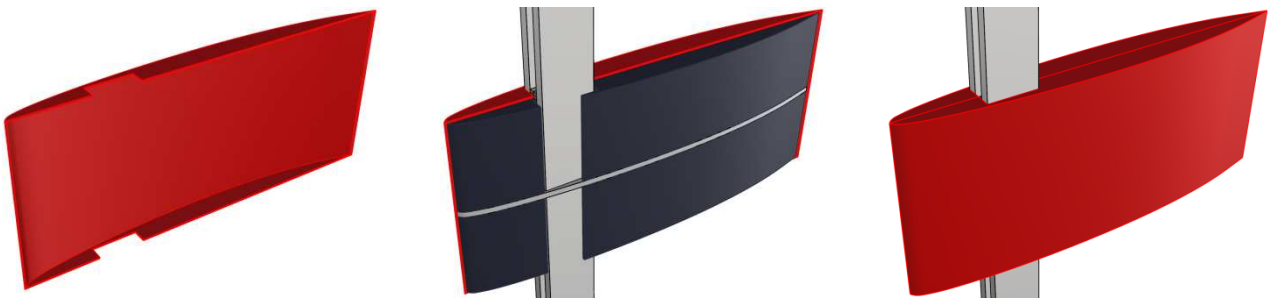


Figure 19. Shell covering of a typical model segment.

The two halves of shell are paired by means of epoxy bonding at model symmetry axis and joined to the perimeter of the beam cross section, which is locally solid, to obtain a watertight case (see Fig. 20).



Figure 20. Detail of H-beam local solid section.

Each segment has a length of 66 mm and it is separated from the adjacent segment by a gap of 1 mm, sufficient to avoid interference of adjacent segments under hydrodynamic loading.

Carbon fibre has been chosen to build the shell, since it allows to realise plates with very good thickness/stiffness ratio.

The spacing between webs and the extension of each case are such as 1 mm of gap is left between each strip.

As already introduced, the ballast should not touch neither the beam nor the shell, and each strip should not touch the neighbouring one : for this reason it is very important to minimise the construction tolerance and implement as much as possible thickness control strategy.

6. CARRIAGE LINK

The experimental tests will be performed at towing tank No.1 of the CNR-INM (Institute of Engineering for Sea) in Rome (Figure 21). The towing tank is 470 m, long 13.5 m wide and has a depth of 6.5 m. It is equipped with a towing carriage that can achieve a maximum speed of 15 m/s.



Figure 21. CNR-INM Towing tank.

The system is arranged vertically with respect to the water surface and connected to the towing carriage with a specially designed connection system. Fig. 22 shows the final arrangement of the hydrofoil beneath the carriage, highlighting its main components. The forces exerted by the fluid will be measured through a three-axis load cell located at the root of the backbone beam (No. 1 item in Fig. 22), while strain-gages are placed along the beam to measure bending deformations. The bar hosting the connection with the wing beam (No.2 item) requires to be much stiffer than the longitudinal H-beam to avoid introducing additional flexibility which may alter the natural frequency of the hydrofoil. An end plate (No.3 item) is present for lowering the free-surface effects on the flow surrounding the hydrofoil.

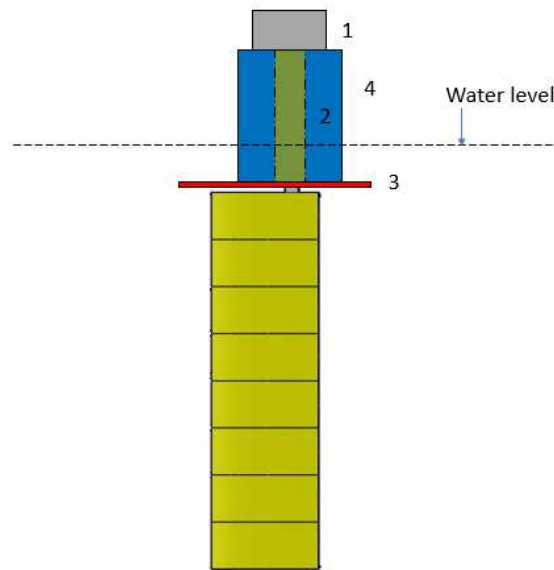


Figure 22. Schematic representation of experimental setup p.

Table 2. Experimental set-up elements.

Number	Element
1	Load cell
2	Link
3	End plate
4	Link cover

All the system represented in Fig. 22 is linked to the towing carriage through a support structure that allows for setting the hydrofoil sinkage, thanks to a motorized telescopic system. This is necessary to compensate variations of the water level in the tank and to achieve the same depth conditions throughout the experimental campaign. A special mechanism also allows for tuning the system yaw to set the hydrofoil incidence to zero on the basis of the load-cell measurements All the data from the sensors will be acquired via the Dewesoft hardware and acquisition software.

7. CONCLUSION

The aim of the present paper is to describe the design procedure of a hydrofoil model to be actually tested for flutter experimental analysis at CNR-INM Institute of Marine Engineering towing tank in Rome, discussing design concept and specifications. The design process is the result of the simultaneous employ of numerical and analytical approaches: CAD models are used for geometrical modelling and mass properties calculations, FEM is employed to calculate model stiffness, natural frequencies and verify model strength, and Theodorsen analytical approach is implemented to predict flutter velocity. A literature review is firstly presented to introduce the chosen reference experimental campaigns. Before discussing the design principles and process, Theodorsen theory is quickly introduced, while deeper attention is paid to discuss the dependency of the flutter speed from the involved physical variables: this was a key step of the design process since it allowed for model optimisation.

The model is designed to encounter flutter at a speed compatible with the range of velocity imposed by the towing tank facility. The combination of design parameters is therefore optimised to meet facility speed range, construction issues and Theodorsen approach application field.

The actual model is designed tightening the limit of Theodorsen theory application: for low value of the ratio between structure and fluid densities, thus for light structure in heavy fluid, the flutter velocity predicted with the analytical model diverges toward infinite. For this reason, one of the driving concept of the design discussed in the present paper, is to maximise the mass of the model, to make the model lying in Theodorsen application field.

The structure of the elastic foil is conceived in a way that the foil flexibility is provided by its elastic backbone beam, while the hydrodynamic load is transferred to the backbone thanks to segmentation of the foil surface. This approach reduces the mutual interaction between components and also guarantees a better analogy with the FEM model and therefore a more rigorous comparison between experimental and numerical results.

The required bending and torsional stiffnesses of the whole model are provided by the H-beam spar running along the foil span, and all the others structural components are assembled avoiding participation to the overall stiffness. The inertial properties are provided by a series of lead ballast blocks, fixed to the structure by means of one aluminium web per model segment. The ballast is defined as *floating* since it does not directly touch neither the beam nor the shell and therefore it is supposed not to add stiffness to the whole structure. The CRP shell has a double purpose: provide external shape and fairing of the profile and making watertight each strip of model.

Natural vibration frequencies of the structure are computed by means of the software ADINA™ solving an eigenvalue modal analysis: transversal (out-of-plane) bending and torsional modes frequencies are needed to feed the Theodorsen's model.

Last but not least, the authors presented a quick overview on the model-to-carriage attachment system and on the planned experimental procedure for determining the flutter velocity.

It can be concluded that when designing a hydrofoil model to be tested experimentally for flutter occurrence at relatively low speed, the dependency of the flutter speed from the mass ratio becomes an issue since it is strongly limited by profile choice, construction and material constrains.

Theodorsen theory was firstly conceived for stability analysis of wings operating in light fluid as the air: the application of this analytical model to light hydrofoils is confirmed to be critical and uncertain.

8. REFERENCES

- Abramson, H. Norman, & Ransleben, G. E. (1965). An experimental investigation of flutter of a fully submerged subcavitating hydrofoil. *Journal of Aircraft*, 2(5), 439–442. <https://doi.org/10.2514/3.43681>
- Abramson, H.N., & Langner, C. G. (1964). *Correlation of various subcavitating hydrofoil flutter predictions using modified oscillatory lift and moment coefficients.*
- ADINA R & D. (2016). Volume I: Solids & Structures. In ADINA R & D (Ed.), *Theory and Modelling Guide ADINA 9.2.*
- Baird, E. F., Squires, C. E. J., & Caporali, R. L. (1962). *INVESTIGATION OF HYDROFOIL FLUTTER - Final Report.*
- Besch, P., & Liu, Y.-N. (1971). *Flutter and divergence characteristics of four low mass ratio hydrofoils* (No. Naval Ship Research and Development Center, Report 3410). Washington D.C.
- Caporali, R. L., & Brunelle, E. J. (1964). Hydrofoil instability at low mass density ratios. *Princeton University, Aerospace and Mechanical Sciences Report 670.*
- Guido Ransleben, E., & Antonio Houston, S. (1970). Experimental determination of variation of hydrofoil flutter speed with mass ratio. In *Southwest Research Institute, SwRI, San Antonio, Houston, USA, Project 02-2584, Final Report Contr. N00014-69-C-0219.* Retrieved from <https://repository.tudelft.nl/islandora/object/uuid%3A5fcac6e0-7960-44be-8e56-7435fcceb089>
- Herr, R. W. (1961). *A Study of Flutter at Low Mass Ratios with Possible Application to Hydrofoils.* Retrieved from https://books.google.it/books?id=jfSxCL_QEWsC
- Kaplan, P., & Lehman, A. F. (1966). An experimental study of hydroelastic instabilities of finite span hydrofoils under cavitating conditions. *AIAA Journal of Aircraft*, 3(3), 262–269. <https://doi.org/10.2514/3.43736>
- Rowe, W. S., & Marvin, T. B. G. (1968). *A PROGRAM OF THEORETICAL RESEARCH ON HYDROELASTIC STABILITY.* The Boeing Company.
- Theodorsen, T. (1935). *Naca-Report-496 General theory of aerodynamic instability and the mechanism of flutter* (No. 496). Washington D.C.
- Theodorsen, T., & Garrick, I. E. (1940). *Naca-Report-685 Mechanism of Flutter, A Theoretical and Experimental Investigation of the Flutter Problem* (No. 685). Retrieved from NACA website: <https://ntrs.nasa.gov/search.jsp?R=19930091762>
- Woolston, D. S., & Castile, G. E. (1951). *Some effects of variations in several parameters including fluid density on the flutter speed of light uniform cantilevered wings* (No. NACA Technical Note No.2558). Washington.
- Wright, J. R., & Cooper, J. E. (2014). Introduction to Aircraft Aeroelasticity and Loads: Second Edition. In *Introduction to Aircraft Aeroelasticity and Loads: Second Edition.* <https://doi.org/10.1002/9781118700440>